Highly Productive C_3H_4/C_3H_6 Trace Separation by a Packing Polymorph of a Layered Hybrid Ultramicroporous Material

Gao, M.-Y.; Bezrukov, A.A.; Song, B.-Q.; He, M.; Nikkhah, S.J.; Wang, S.-Q.; Kumar, N.; Darwish, S.; Sensharma, D.; Deng, C.; Li, J.; Liu, L.; Krishna, R.; Vandichel, M.; Yang, S.; Zaworotko, M.J.

DOI
10.1021/jacs.3c03505

Publication date
2023

Document Version
Final published version

Published in
Journal of the American Chemical Society

JACS
JOURNAL OF THE AMERICAN CHEMICAL SOCIETY
pubs.acs.org/JACS
Article

Highly Productive C_3H_4/C_3H_6 Trace Separation by a Packing Polymorph of a Layered Hybrid Ultramicroporous Material

Mei-Yan Gao, Andrey A. Bezrukov, Bai-Qiao Song, Meng He, Sousa Javan Nikkhah, Shi-Qiang Wang, Naveen Kumar, Shaza Darwish, Debobroto Sensharma, Chenghua Deng, Jiangnan Li, Lunjie Liu, Rajamani Krishna, Matthias Vandichel, Sihai Yang, and Michael J. Zaworotko*

Cite This: J. Am. Chem. Soc. 2023, 145, 11837−11845
Read Online

ACCESS | Metrics & More | Article Recommendations | Supporting Information

ABSTRACT: Ultramicroporous materials can be highly effective at trace gas separations when they offer a high density of selective binding sites. Herein, we report that **sql-NbOFFIVE-bpe-Cu**, a new variant of a previously reported ultramicroporous square lattice, **sql**, topology material, **sql-SIFSIX-bpe-Zn**, can exist in two polymorphs. These polymorphs, **sql-NbOFFIVE-bpe-Cu-AA** (**AA**) and **sql-NbOFFIVE-bpe-Cu-AB** (**AB**), exhibit AAAA and ABAB packing of the **sql** layers, respectively. Whereas **NbOFFIVE-bpe-Cu-AA** (**AA**) is isostructural with **sql-SIFSIX-bpe-Zn**, each exhibiting intrinsic 1D channels, **sql-NbOFFIVE-bpe-Cu-AB** (**AB**) has two types of channels, the intrinsic channels and extrinsic channels between the **sql** networks. Gas and temperature induced transformations of the two polymorphs of **sql-NbOFFIVE-bpe-Cu** were investigated by pure gas sorption, single-crystal X-ray diffraction (SCXRD), variable temperature powder X-ray diffraction (VT-PXRD), and synchrotron PXRD. We observed that the extrinsic pore structure of **AB** resulted in properties with potential for selective C_3H_4/C_3H_6 separation. Subsequent dynamic gas breakthrough measurements revealed exceptional experimental C_3H_4/C_3H_6 selectivity (270) and a new benchmark for productivity (118 mmol g^{-1}) of polymer grade C_3H_6 (purity >99.99%) from a 1:99 C_3H_4/C_3H_6 mixture. Structural analysis, gas sorption studies, and gas adsorption kinetics enabled us to determine that a binding "sweet spot" for C_3H_4 in the extrinsic pores is behind the benchmark separation performance. Density-functional theory (DFT) calculations and Canonical Monte Carlo (CMC) simulations provided further insight into the binding sites of C_3H_4 and C_3H_6 molecules within these two hybrid ultramicroporous materials, HUMs. These results highlight, to our knowledge for the first time, how pore engineering through the study of packing polymorphism in layered materials can dramatically change the separation performance of a physisorbent.

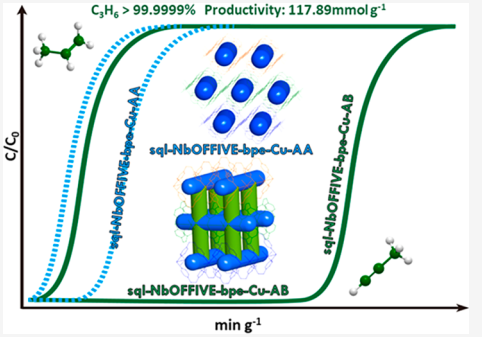

INTRODUCTION

Metal−organic materials (MOMs)[1] such as metal−organic frameworks (MOFs)[2−4] and porous coordination polymers (PCPs)[5] are of topical interest because of their potential utility in, for example, gas storage, catalysis, biochemical imaging, and drug delivery.[6−9] With respect to design, the diversity of their structures and compositions makes MOMs amenable to crystal engineering,[10] which can enable systematic tuning of composition to control pore size, shape, and chemistry, *i.e.* "pore engineering".[11−15] Established approaches to pore engineering include interpenetration, flexibility, open metal sites (OMSs), functionalized ligands, counterion substitution, and pore space partition, which tend to lower pore volume.[15−17] To our knowledge, pore engineering by different packing of adjacent layers, i.e. polymorphism, has not yet been reported.

Hybrid ultramicroporous materials (HUMs), a subclass of MOMs, are based on inorganic pillars such as MFSIX (e.g., GeF_6^{2-}, TiF_6^{2-}, SiF_6^{2-}, SnF_6^{2-}), FOXY (e.g., $NbOF_5^{2-}$), and M'FFIVE (e.g., AlF_5^{2-}, FeF_5^{2-}). HUMs are of topical interest thanks to their strong and selective binding interactions with small gas molecules including CO_2 and hydrocarbons (HCs).[18−26,11,20,27−37] Most HUMs are based on rigid organic linkers (e.g., pyrazine, 4,4′-bipyridine) and pillared by inorganic anions to afford three-dimensional rigid networks. Whether interpenetration of the networks occurs depends mainly on the length and rigidity of linker ligands (Table S2).[18,19,21−23,38−40] Flexible linker ligands, e.g. 4,4′-dipyridylsulfide (dps), 4,4′-dipyridylsulfone, 4,4′-dipyridylsulfoxide, 1,2-bis(4-pyridyl)-ethane (bpe), and 1,3-bis(4-pyridyl)propane (bpp), have the potential to form spiro-linked 1D coordination polymers that, when pillared by inorganic anions, afford 2D square lattice (**sql**) coordination networks (Scheme 1 and Table S3).[24,27,41−44] **sql-SIFSIX-bpe-Zn**, SIFSIX = SiF_6^{2-}, exemplifies such structures

Received: April 4, 2023
Published: May 19, 2023

https://doi.org/10.1021/jacs.3c03505
J. Am. Chem. Soc. 2023, 145, 11837−11845

Scheme 1. Rigid Linker Ligands Tend to Generate sql Topology Coordination Networks (Above) Whereas Flexible Linkers Can Afford Either sql Networks or Spiro-Linked 1D Coordination Polymers (Below)

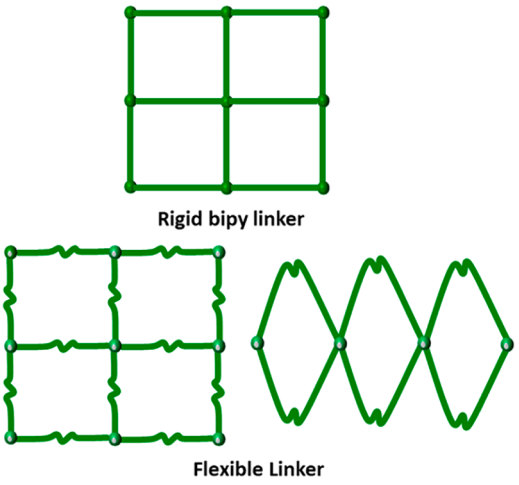

and was reported to exhibit high binding affinity for C_2H_2 via an induced fit mechanism enabled by flexibility.[27]

Herein, we report that solvent-mediated crystallization can result in packing polymorphs of the related material **sql-NbOFFIVE-bpe-Cu**, **sql-NbOFFIVE-bpe-Cu-AA**, **AA**, and **sql-NbOFFIVE-bpe-Cu-AB**, **AB**, which exhibit AAAA and ABAB packing of their **sql** layers, respectively, and study the effect of crystal packing upon the C3 sorption properties of **sql-NbOFFIVE-bpe-Cu**. C3 sorption is relevant because propylene (C_3H_6) is a feedstock for the production of commodity chemicals such as acrylonitrile, propylene oxide, and polypropylene.[45−47] Worldwide propylene production capacity was as high as 140 million tons in 2020, second only to that of ethylene among chemical building blocks.[13] Further purification of C_3H_6 is needed because trace amounts (∼1%) of propyne (C_3H_4) must be removed to afford polymer-grade (≥99.95%) C_3H_6 for downstream applications.[38,48] That C_3H_4 and C_3H_6 exhibit similar physicochemical properties (Scheme 2 and Table S1)[49] makes it a challenge for porous materials to produce polymer-grade C_3H_6. The C3 sorption properties of **AA** and **AB** are addressed through a series of experimental and computational studies.

Scheme 2. Comparison of the Molecular Structures and Physical Properties of C_3H_4 and C_3H_6

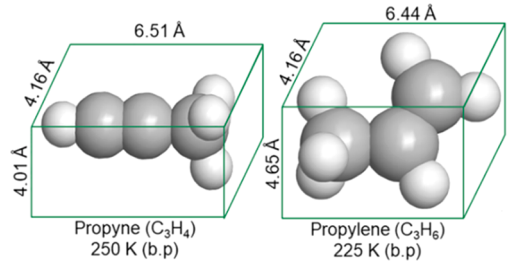

EXPERIMENTAL SECTION

All reagents and solvents were purchased commercially and used as received without further purification, except the precursor $CuNbOF_5 \cdot 4H_2O$, which was prepared by adapting a reported procedure.[50]

Synthesis of pcu-NbOFFIVE-bpe-Cu ($[Cu(NbOF_5)(bpe)_2]_n$). In a typical reaction, bpe (6.3 mg, 0.035 mmol) in 2 mL of methanol was carefully layered onto $CuNbOF_5 \cdot 4H_2O$ (7 mg, 0.026 mmol) in 2 mL of water. Blue block single crystals were obtained after 4 days in quantitative yield, collected by filtration and washed with methanol three times.

Synthesis of sql-NbOFFIVE-bpe-Cu-AA-α, AA-α, ($[Cu(NbOF_5)(bpe)_2]_n$). In a typical reaction, $CuNbOF_5 \cdot 4H_2O$ (0.0345 g, 0.13 mmol) and bpe (0.0276 g, 0.15 mmol) were added to 11.0 mL of H_2O/CH_3OH (v/v = 9:2). The solution was then sealed in a 14.5 mL vial and settled for 1 h. A light blue powder was obtained. This reaction can be readily scaled. When the reaction was conducted at room temperature or 60 °C for 2 months, blue block crystals of **AA-α** were obtained which were suitable for single-crystal X-ray diffraction (SCXRD) testing.

Preparation of sql-NbOFFIVE-bpe-Cu-AA-β, AA-β. A single crystal of the methanol exchanged phase of **AA-α** was activated at 333 K *in situ* on the goniometer of an SCXRD instrument. After 10 min SCXRD data showed that **AA-α** had transformed to **AA-β**. Bulk samples were prepared through activation at 333 K under vacuum.

Synthesis of sql-NbOFFIVE-bpe-Cu-AB-α, AB-α, ($[Cu(NbOF_5)(bpe)_2]_n$). In a typical reaction, a solution of $CuNbOF_5 \cdot 4H_2O$ (7 mg, 0.026 mmol) in 1 mL of water was carefully layered onto bpe (6.3 mg, 0.035 mmol) in 4 mL of 1,2-dichlorobenzene. Block shaped dark blue single crystals of **AB-α** were obtained after 3 days. The crystals were collected by filtration and washed with methanol three times, yield 85%.

Preparation of sql-NbOFFIVE-bpe-Cu-AB-β_1, AB-β_1. Methanol exchanged **AB-α** was activated by heating at 333 K under vacuum for 12 h and then exposed to air or soaked in water to yield **AB-β_1**.

RESULTS AND DISCUSSION

Solvent diffusion of $CuNbOF_5 \cdot 4H_2O$ and bpe in various organic solvents and water at room temperature afforded single crystals of three polymorphs of $[Cu(NbOF_5)(bpe)_2]_n$: a 3D **pcu** network; two 2D **sql** networks. When using 1:1 H_2O/CH_3OH (v/v), single crystals of the 3D **pcu** network, **pcu-NbOFFIVE-bpe-Cu**, were obtained with bulk purity (Figures 1 and S12).

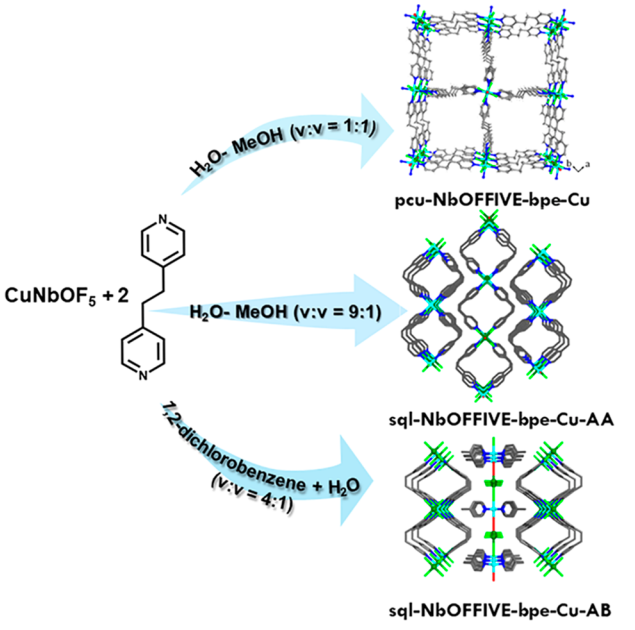

Figure 1. Synthetic conditions used and crystal structures of **pcu-NbOFFIVE-bpe-Cu**, **sql-NbOFFIVE-bpe-Cu-AA-α**, and **sql-NbOFFIVE-bpe-Cu-AB-α**. Color code: turquoise, Cu; green, Nb; red, O; bright green, F; blue, N; gray, C. Hydrogen atoms are omitted for clarity.

https://doi.org/10.1021/jacs.3c03505
J. Am. Chem. Soc. 2023, 145, 11837−11845

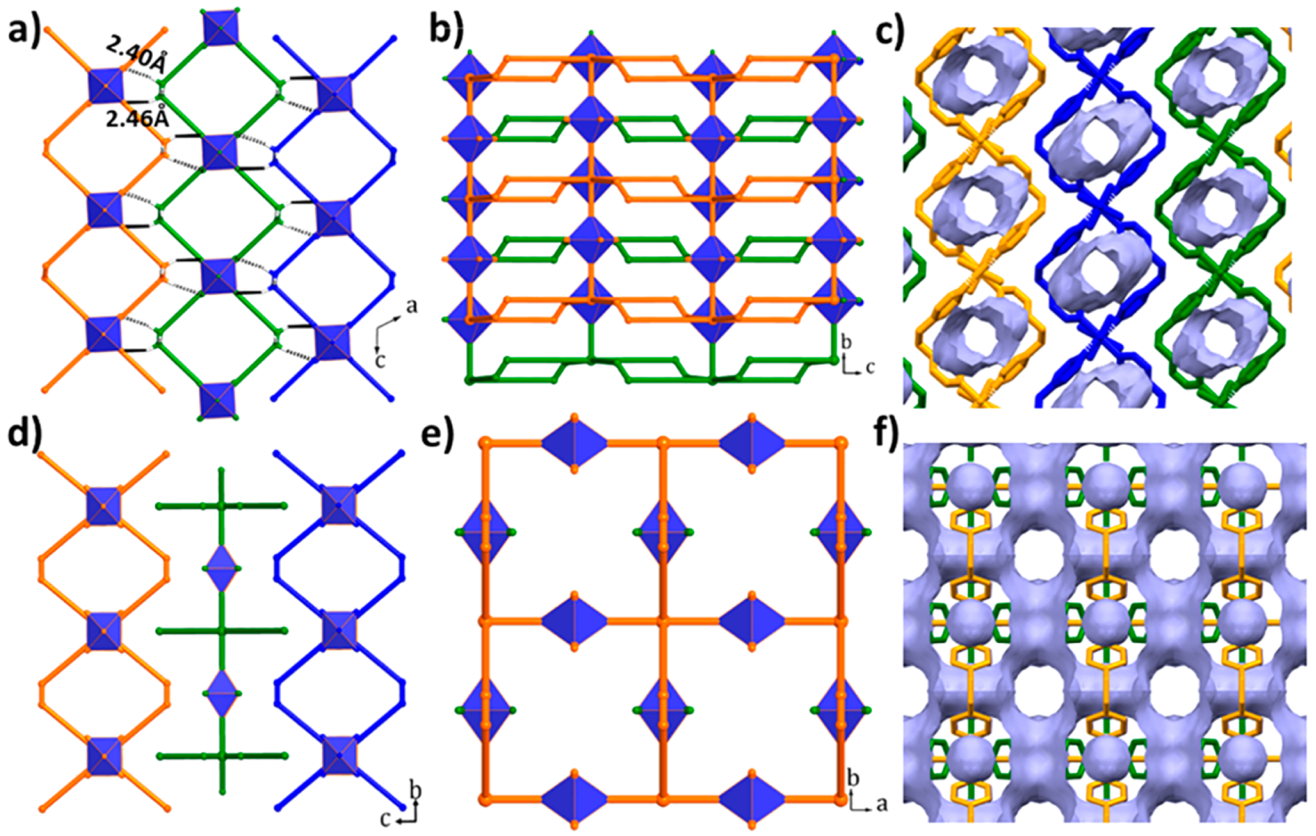

Figure 2. Comparisons of **sql-NbOFFIVE-bpe-Cu-AA-*α*** (a, b, c) and **sql-NbOFFIVE-bpe-Cu-AB-*α*** (d, e, f). Simplified crystal structure of **sql-NbOFFIVE-bpe-Cu-AA-*α*** along the b (a) and a axes (b); (c) 1D channels in **sql-NbOFFIVE-bpe-Cu-AA-*α***; Simplified crystal structures of **sql-NbOFFIVE-bpe-Cu-AB-*α*** along the a (d) and c axes (e); (f) 3D channels in **sql-NbOFFIVE-bpe-Cu-AB-*α***. Color code: blue = $NbOF_5$; black = hydrogen bonds; Adjacent layers colored orange, green, and blue. Hydrogen atoms omitted for clarity.

SCXRD revealed that **pcu-NbOFFIVE-bpe-Cu** had crystallized in the tetragonal space group *P*4/*n* (Table S4). The non-interpenetrated network exhibits ~9 × 9 Å pores, but crystals of **pcu-NbOFFIVE-bpe-Cu** did not survive guest removal, making it a first generation porous coordination polymer as classified by Kitagawa and co-workers (Figure S3).[5] When the ratio of H_2O/CH_3OH was changed to 9:2 (v/v), single crystals of a 2D **sql** network variant, **AA-*α***, were isolated (Figures 1, S1 and S5 upper). SCXRD analysis revealed that **AA-*α*** had crystallized in the monoclinic space group *C*2/*c* (Table S4). A 4:1 ratio of 1,2-dichlorobenzene and water (v/v) afforded single crystals of a polymorph of the same **sql** network, **AB-*α*** (Figures 1, S2, and S5 lower). SCXRD analysis revealed that **AB-*α*** had crystallized in tetragonal space group $P4_2/mmc$ (Table S5). Bulk purities of **AA-*α*** and **AB-*α*** were confirmed by powder X-ray diffraction (PXRD, Figure S13).

Each Cu^{2+} cation in **AA-*α*** and **AB-*α*** is six-coordinate, coordinated by four N atoms from bpe ligands as well as one O atom and one F atom from two $NbOF_5^{2-}$ anions (Figure S4). The pyridyl moieties are oriented in a *gauche* conformation about the C−C single bond backbone, resulting in a V-shaped bis(monodentate) linking mode. The layers in **AB-*α*** and **AA-*α*** stack differently. **AA-*α*** formed an AAAA layer arrangement similar to other **sql** topology HUMs (Figures 2, S5, and S6, some presented using simplified structures).[11,24,27,41−44,51] Adjacent layers form H-bonds C(bpe ligand)−H···F($NbOF_5$) of 2.40 and 2.46 Å that result in an arrangement reminiscent of a zipper. With respect to **AB-*α***, $NbOF_5^{2-}$ anion pillared $Cu(bpe)_2$ chains along the *a*-axis and *b*-axis lie in the *ab*-plane (Figures S5 and S7). **AB-*α*** was found to exhibit ABAB stacking of layers, resulting in a pore structure distinct from that of **AA-*α*** and related materials.[27] The resulting ultramicroporous channels (3.96 × 5.56 $Å^2$, after subtracting the van der Waals radii, Figure 2f) represent 29.9% of the unit cell volume as calculated by PLATON.[52] The 1D channels in **AA-*α*** resulted in a solvent-accessible space of 24.7% of the unit cell volume (Figure 2c). We anticipated that the inherent flexibility of bpe might enable induced fit or preferential binding toward C_3H_4 over C_3H_6[10] and that the electronegative $NbOF_5^{2-}$ anions lining the channels might preferentially bind alkynes vs alkenes (Figure 2c and 2f).[24,42,53−56] We therefore undertook a study of the separation performance of these polymorphs toward C_3H_4 and C_3H_6.

As-synthesized **AB-*α*** transformed to a narrower-pore phase, **AB-*β***, after methanol exchange at 333 K under vacuum for 12 h. We were unable to directly determine the crystal structure of activated (anhydrate) **AB-*β***, as it captured water from air at low relative humidity (RH), as revealed by dynamic vapor sorption (DVS) (Figure S26). Figures S27 and S28 reveal that water vapor was adsorbed within minutes at 30% RH, 298 K. The SCXRD structure determined in air, **AB-*β*$_1$**, was found to be a hydrate with twisted pores, twisted $NbOF_5^{2-}$ anions, and undulating pillars, unlike **AB-*α*** (Figure S9). TGA data collected after holding at 80 °C for 2 h revealed no weight loss, further indicating that **AB-*β*** is fully activated and that water vapor was captured from the laboratory atmosphere (Figure S18). **AB-*β*$_1$** crystallized in the tetragonal space group $P4_2/mnm$ (Table S5). The distance between F atoms ($d_{F\cdots F}$) in adjacent pillars changed from 6.33 Å in **AB-*α*** to 6.91 and 5.37 Å in **AB-*β*$_1$** (Figure S10).

https://doi.org/10.1021/jacs.3c03505
J. Am. Chem. Soc. 2023, 145, 11837−11845

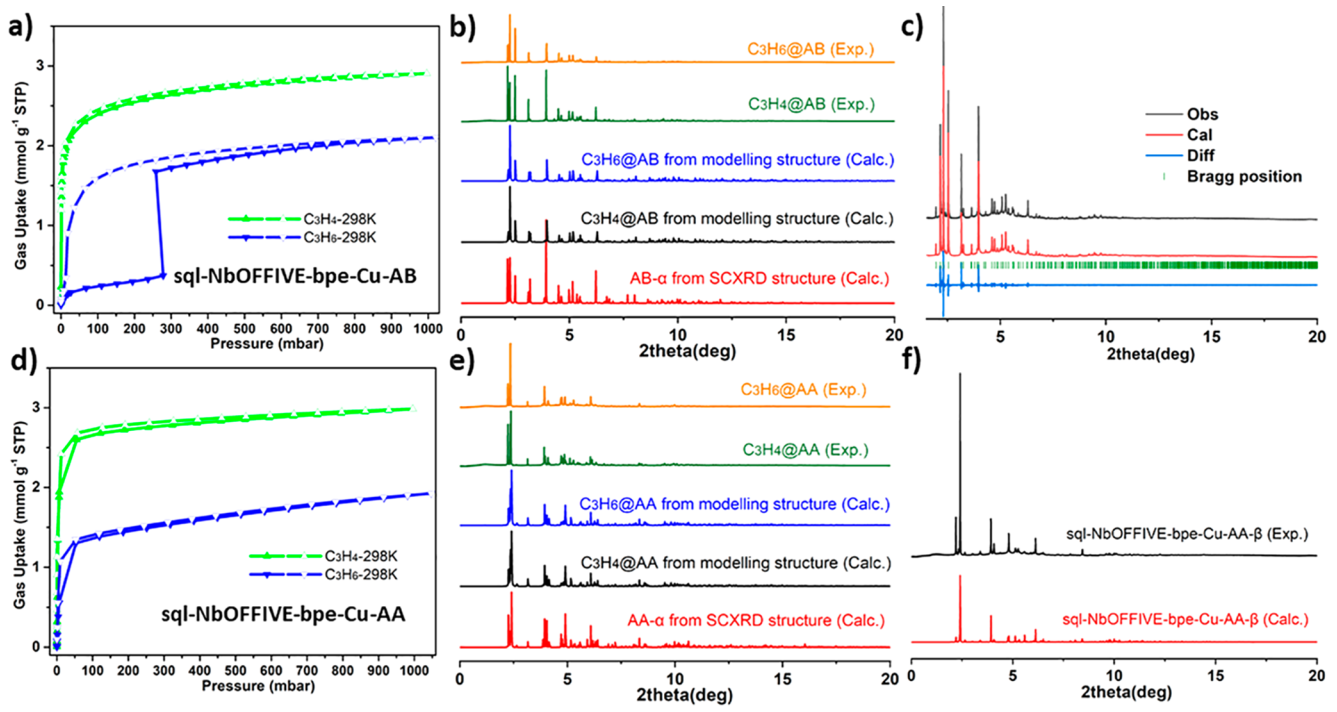

Figure 3. (a) C_3H_4 and C_3H_6 adsorption isotherms of **sql-NbOFFIVE-bpe-Cu-AB** collected at 298 K; (b) S-PXRD (λ = 0.35424308 Å) patterns of C_3H_4-loaded and C_3H_6-loaded **sql-NbOFFIVE-bpe-Cu-AB-*α*** compared with the PXRD patterns calculated from SCXRD and modeling data; (c) Pawley profile fit for **sql-NbOFFIVE-bpe-Cu-AB-*β***. The experimental S-PXRD data are presented in black, calculated in red, and the difference between experimental and calculated in blue. Bragg reflections are shown as green bars. Crystal system = Tetragonal, Space group = $P4_2/mnm$, $a = b$ = 12.4888(4) Å, c = 18.8761(6) Å, V = 2944.1(2) Å^3, r_wp = 3.216%, r_exp = 1.821%, r_p = 3.127%, GOF = 1.766; (d) C_3H_4 and C_3H_6 adsorption isotherms of **sql-NbOFFIVE-bpe-Cu-AA** at 298 K; (e) S-PXRD (λ = 0.35424308 Å) patterns of C_3H_4-loaded and C_3H_6-loaded **sql-NbOFFIVE-bpe-Cu-AA-*α*** compared with their corresponding PXRD patterns calculated from SCXRD and modeling data; (f) S-PXRD patterns of experimental **sql-NbOFFIVE-bpe-Cu-AA-*β*** compared with calculated PXRD of **sql-NbOFFIVE-bpe-Cu-AA-*β*** from SCXRD.

Activation of **AA-*α*** resulted in **AA-*β***. Heating at 333 K *in situ* on the SCXRD goniometer enabled structural determination of **AA-*β*** (Figure S8), which had crystallized in the monoclinic space group $I2/m$ (Table S4). The $d_{F\cdots F}$ value decreased from 7.1104 Å in **AA-*α*** to 6.9260 Å in **AA-*β*** (Figure S11).

These transformations were also investigated by variable-temperature PXRD (VT-PXRD). **AA-*α*** converted to **AA-*β*** by heating at 333 K under N_2, the PXRD pattern matching that calculated from the SCXRD structure (Figure S16a). Methanol exchanged **AB-*α*** transformed to desolvated **AB-*β*** after heating at 393 K under N_2 (Figure S16b). Methanol exchanged **AB-*α*** can also transform to **AB-*β*** by heating at 333 K under vacuum for 6 h (Figure S16c). The partially loaded **AB-β_1** phase was also observed by VT-PXRD at 333 K, its PXRD diffractogram matching the calculated PXRD pattern of **AB-β_1**. **AB-*β*** was observed to transform to **AA-*β*** after heating at 473 K under N_2 (Figure S16b).

To investigate the porosity of **AA** and **AB**, gas sorption isotherms of CO_2, at 195 K, and N_2, at 77 K, were collected (Figure S19). Prior to collection of sorption data, methanol exchanged **AA** and **AB** were activated at 333 K for 12 h under vacuum to generate their respective ***β*** forms. CO_2 adsorption by **AB** revealed a stepped isotherm profile with an inflection at low pressure (ca. 0.024 bar) and an uptake of ca. 1.5 mmol g^{-1} after the first step.[57] A saturated CO_2 uptake of ∼2.9 mmol g^{-1} corresponds to almost 4 CO_2 molecules per unit cell. In the case of N_2 adsorption, an uptake of ∼2.0 mmol g^{-1} was observed. The corresponding values for **AA** revealed CO_2 and N_2 uptakes of ∼3.5 mmol g^{-1} and ∼1.0 mmol g^{-1}, respectively. Langmuir surface areas of 356 m^2 g^{-1} for **AA** and 295 m^2 g^{-1} for **AB** were calculated from 195 K CO_2 isotherms. The maximum pore size distributions derived from 195 K CO_2 data were determined to be 3.55 for **AA** and 6.04 Å for **AB**, matching the pore sizes derived from SCXRD data (Figure S19). For a larger probe size, such as N_2 at 77 K (3.6 Å for N_2 vs 3.3 Å for CO_2), **AA** shows lower uptake than that of **AB** because of its narrower pore.

Next, we studied the C_3H_4 and C_3H_6 adsorption properties of **AB** and **AA** at 273 and 298 K (Figures 3a, 3d, S20, and S21). The C_3H_4 sorption isotherm of **AB** revealed steep uptake at low pressure and an uptake of 3.04 mmol g^{-1} at 1 bar and 298 K, significantly higher than its C_3H_6 uptake (2.10 mmol g^{-1}) under the same conditions. We note that the uptake of C_3H_6 was negligible at low pressure (0.01 mmol g^{-1} at 0.001 bar; 0.1 mmol g^{-1} at 0.01 bar; 0.23 mmol g^{-1} at 0.1 bar), reflecting the stepped sorption isotherm.[57] The corresponding C_3H_4 uptakes were higher (1.20 mmol g^{-1} at 0.001 bar; 1.93 mmol g^{-1} at 0.01 bar; 2.40 mmol g^{-1} at 0.1 bar, Figure S21). Similar stepped isotherms were reported for GEFSIX-dps-Cu, ELM-12, and ZU-13.[11,58,59] The uptake ratio of C_3H_4/C_3H_6 for **AB** at 1 mbar is higher than that of NKMOF-11.[12] Sample regeneration was realized by exposure to vacuum at 333 K for as little as 10 min. Multiple sorption tests were performed, and similar sorption isotherms were observed, indicating good recyclability (Figure S22).

The differences between the single-component isotherms of C_3H_4 and C_3H_6 are indicative of potential utility for separation of C_3H_4/C_3H_6 binary mixtures. In the case of **AA**, the uptake ratio of C_3H_4/C_3H_6 at 1 mbar (∼3.8) is much lower than that of **AB** (∼120), although **AA** shows a similar uptake of C_3H_4 at 1 bar and lower uptake of C_3H_6 than **AB** (Figure S21). These results

https://doi.org/10.1021/jacs.3c03505
J. Am. Chem. Soc. 2023, 145, 11837−11845

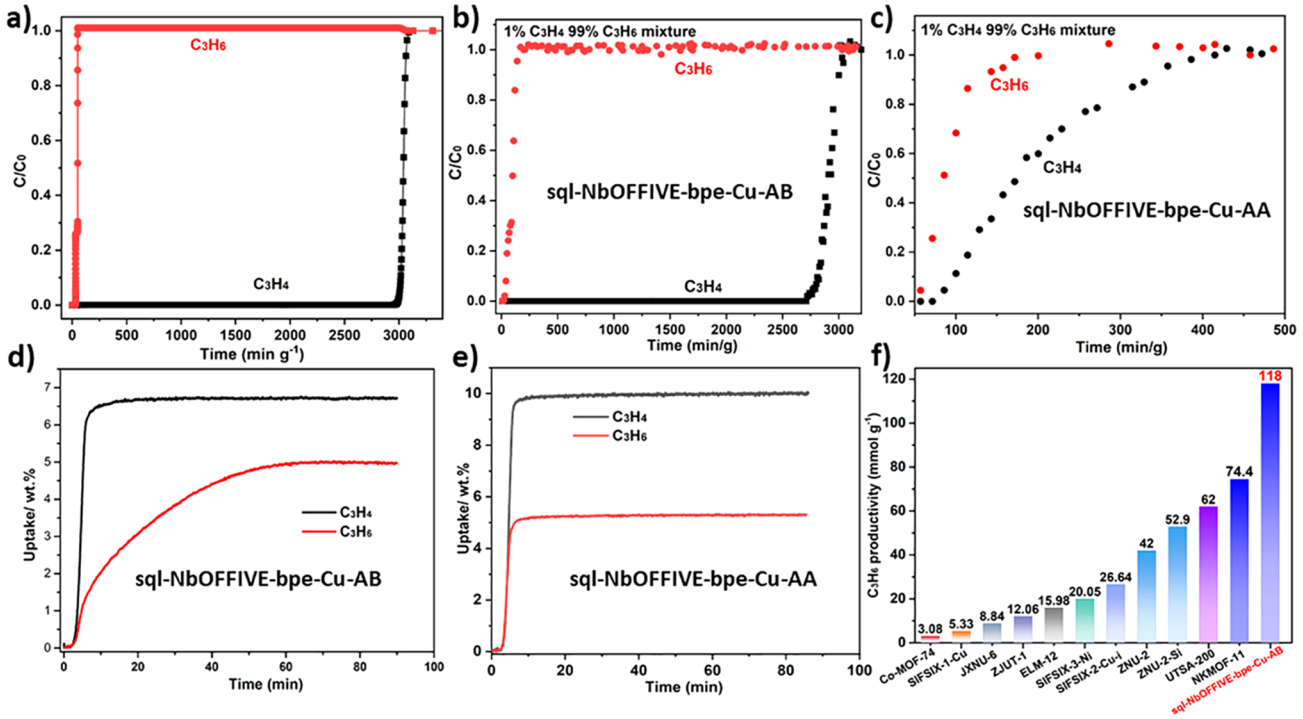

Figure 4. (a) Simulated breakthrough curves of **sql-NbOFFIVE-bpe-Cu-AB** for separation of C_3H_4/C_3H_6 (1/99) mixture at 298 K; (b) Experimental breakthrough separation of **sql-NbOFFIVE-bpe-Cu-AB** for C_3H_4/C_3H_6 (1/99) at 298 K (gas velocity: 1.0 cm^3 min^{-1}); (c) Experimental breakthrough separation of **sql-NbOFFIVE-bpe-Cu-AA** for C_3H_4/C_3H_6 (1/99) at 298 K (gas velocity: 1.0 cm^3 min^{-1}); (d) Gravimetric kinetics of **sql-NbOFFIVE-bpe-Cu-AB** for C_3H_4 and C_3H_6 uptake (0−1.0 bar) at 303 K; (e) Gravimetric kinetics of **sql-NbOFFIVE-bpe-Cu-AA** for C_3H_4 and C_3H_6 uptake (1.0 bar) at 303 K; (f) Comparison of C_3H_6 productivity in representative benchmark materials for separation of 1/99 C_3H_4/C_3H_6 mixture.

indicate that **AB** offers stronger potential for separation of C_3H_4/C_3H_6 than **AA**.

Synchrotron PXRD (S-PXRD) data were collected for activated as well as C_3H_4 and C_3H_6-loaded samples to study the guest-induced structural change. As shown in Figure 3b and 3e, S-PXRD diffractograms of C_3H_4 and C_3H_6-loaded **AA** and **AB** support the presence of the corresponding ***α*** phases. The S-PXRD pattern of activated **AA-*β*** obtained by heating at 333 K under vacuum is consistent with the calculated pattern (Figure 3f). Pawley fitting for **AB-*β*** revealed tetragonal space group $P4_2/mnm$ (Figure 3c) and a unit cell volume of **AB-*β*** (2944.1(2) $Å^3$) slightly smaller than that of **AB-β_1** (2954.6(4) $Å^3$). These results indicate that both C_3H_4 and C_3H_6 can induce phase changes from the narrow-pore phases (**AA-*β*** and **AB-*β***) to the respective open phases (**AA-*α*** and **AB-*α***).

To quantify the potential of **AB** for separation of the challenging C_3H_4/C_3H_6 binary mixtures, ideal adsorption solution theory (IAST) calculations were conducted using Dual-site Langmuir−Freundlich (DSLF) and 3-site Langmuir−Freundlich isotherm shape models[60−62] (Figures S23 and S24, Tables S6 and S7). The calculated adsorption selectivity values for 1:99 and 1:1 C_3H_4/C_3H_6 binary mixtures are up to 220 and over 180 at 298 K and 1 bar, respectively. Simulated breakthrough data using a methodology described previously predicts excellent separation performance for C_3H_4/C_3H_6 (Figure 4a).[63−67]

In order to experimentally evaluate the C_3H_4/C_3H_6 separation performance of **AA** and **AB**, we conducted dynamic column breakthrough (DCB) experiments that mimic typical process conditions with an inlet gas mixture composition of 1:99 (v/v) C_3H_4/C_3H_6.[12,22] This C_3H_4/C_3H_6 gas mixture with a flow rate of 1.0 cm^3 min^{-1} was passed through a fixed bed column (8 mm diameter) packed with sorbent at 1 bar and 298 K. The fixed beds of methanol exchanged samples were first activated by heating at 353 K in a 20 cm^3 min^{-1} flow of Helium for about 6 h. DCB experiments were commenced after samples were cooled to room temperature. Gas chromatography (GC) was used to monitor eluted components quantitatively at short sampling intervals (Figure S29; see Supporting Information for the experimental setup). As expected (Figure 4b and 4c), **AB** was indeed found to be more effective for C_3H_4/C_3H_6 separation than **AA**. For **AB**, C_3H_6 breakthrough occurred at 10 min g^{-1}, well before C_3H_4 (2710 min g^{-1}). This represents a C_3H_4 uptake capacity (1.2 mmol g^{-1}, Table S8) comparable to that of the previous benchmark sorbent, NKMOF-1-Ni (1.21 mmol g^{-1}) and Ni@FAU (1.59 mmol g^{-1}).[49,68] During the time lag of 2710 min g^{-1} before breakthrough, GC data showed that the concentration of C_3H_4 in the effluent gas stream was <1 ppm (Table S8). According to the DCB profile obtained from a 1/99 mixture, the polymer-grade C_3H_6 productivity (>99.99% purity) of **AB** sets a new benchmark value of 118 mmol g^{-1}, beyond that of previous benchmark materials (NKMOF-11, 74.4 mmol g^{-1}; UTSA-200, 62.0 mmol g^{-1}; ZNU-2-Si, 52.9 mmol g^{-1}; ZNU-2, 42 mmol g^{-1}; SIFSIX-3-Ni, 20.05 mmol g^{-1} and SIFSIX-2-Cu-i, 26.64 mmol g^{-1}, Figure 4f).[12,13,38,48,69] Separation selectivity (α_{AC}) was calculated to be 270, exceeding that of reported HUMs with **sql** topology GeFSIX-dps-Cu (82.1), GeFSIX-dps-Zn (65.6).[11] That **AB** outperformed previous benchmark materials in terms of C_3H_6 productivity demonstrates that HUMs can offer both high selectivity and high uptake for challenging gas separations.

https://doi.org/10.1021/jacs.3c03505
J. Am. Chem. Soc. 2023, 145, 11837−11845

We also studied the pure gas adsorption kinetics for C_3H_4 and C_3H_6 using methanol exchanged samples, whereby activated samples of **AA** and **AB** were exposed to a constant flow of 10 cm^3 min^{-1} C_3H_4 and C_3H_6 at 303 K and 1.0 bar. As presented in Figure 4d, the slope of the kinetic curve for **AB** is much steeper for C_3H_4 than that of C_3H_6, indicating faster adsorption kinetics for C_3H_4. The kinetic curves of C_3H_4 and C_3H_6 level off at 6.8 wt % (1.7 mmol g^{-1}) after ca. 10 min and 2.5 wt % (1.2 mmol g^{-1}) after ca. 60 min, respectively. Regeneration tests were performed by heating the samples at 353 K under N_2 flow for ca. 1 h (flow rate: 60 cm^3 min^{-1}), and no changes in uptake were observed after successive cycles (Figure S25). With respect to **AA**, the slope of the kinetic curve is almost the same for C_3H_4 and C_3H_6, indicating similar adsorption kinetics for C_3H_4 and C_3H_6 (Figures 4e and S25). That gas adsorption kinetics in **AB** favors C_3H_4 over C_3H_6 is desirable for efficient gas separation during dynamic DCB tests.

Hydrolytic stability of a sorbent is a prerequisite for utility, prompting us to soak crystals of **AB** in water and perform water vapor sorption experiments using DVS. The water sorption experiment revealed a type I isotherm with approximately 15 wt % uptake at about 90% RH, which is consistent with the weight loss observed in the TGA curve (~12 wt %, Figures S17 and S26). Cycling tests were performed 10 times and revealed that the sample retained stability when exposed to humidity (Figure S28). Crystals soaked in water for 5 days retained crystallinity (Figure S14).

Insight into the distinct sorption properties of **AA** and **AB** was gained through DFT calculations, which revealed that **AA** and **AB** have similar lattice energies, the **AB** to **AA** transformation being predicted to be exothermic by −13.2 kJ mol^{-1} per $Cu_2Nb_2O_2F_{10}(bpe)_4$ formula unit. DFT was also used to identify the most plausible binding sites and their adsorption enthalpies whereas Canonical Monte Carlo (CMC) simulations were conducted to obtain adsorbate occupancy or the density map comprising the binding site regions (see Supporting Information for further details on the computational methodology). For each framework, the energetically most plausible orientations for C_3H_4 and C_3H_6 are represented in Figure 5. The binding sites were identified using DFT calculations in which atomic positions were optimized so that the binding pockets can adapt to each adsorbate.

The resulting adsorption enthalpies C_3H_4 and C_3H_6 in **AA** were calculated to be −62.7 (C_3H_4) and −65.2 (C_3H_6) kJ mol^{-1}, respectively. These similar adsorption enthalpies and Gibbs free energy differences are indicative of poor selectivity for C3 hydrocarbons. These values are also in line with experimental data (Figure 4c). In contrast, the adsorption enthalpies of −69.0 (C_3H_4) and −53.0 (C_3H_6) kJ mol^{-1} calculated for **AB** suggest enhanced binding of C_3H_4 and weaker C_3H_6 binding compared to **AA**, also in line with experimental observations (Figure 4b). The 16 kJ mol^{-1} difference in adsorption enthalpy for **AB** is also found in the adsorption Gibbs free energy differences ΔG_{ads} of −24.4 (C_3H_4) and −8.5 (C_3H_6) kJ mol^{-1}, where a difference of only 4.4 kJ mol^{-1} was calculated for **AA**, with ΔG_{ads} values of −19.6 (C_3H_4) and −15.0 (C_3H_6) kJ mol^{-1}, respectively. For both adsorbates, there are hydrogen bonds between H atoms of the adsorbates and framework F atoms (Figure 5), as is typical for HUMs.[70−73] A detailed analysis of these binding sites, including adsorption energy and distances, is summarized in Table S9. Binding site isosurfaces from CMC simulations are visualized in Tables S11 and S12 and reveal that the density fields, comprising adsorbate mass-middle point occupancies of successful insertion moves, of C_3H_4 are larger than those of C_3H_6 for all frameworks. This can be attributed to the more linear geometry of C_3H_4 resulting in a larger binding area. Furthermore, the CMC results validate the preferred positions of the adsorbates in the framework and its channels in the vicinity of framework F atoms, which can be observed by merging the binding site outcomes from DFT and CMC (Figures S31 and S32). The four modeled crystal structures were used to calculate PXRD patterns, which are a good match for both the experimental S-PXRD data and the PXRD patterns calculated from SCXRD data (Figure 3b, 3e).

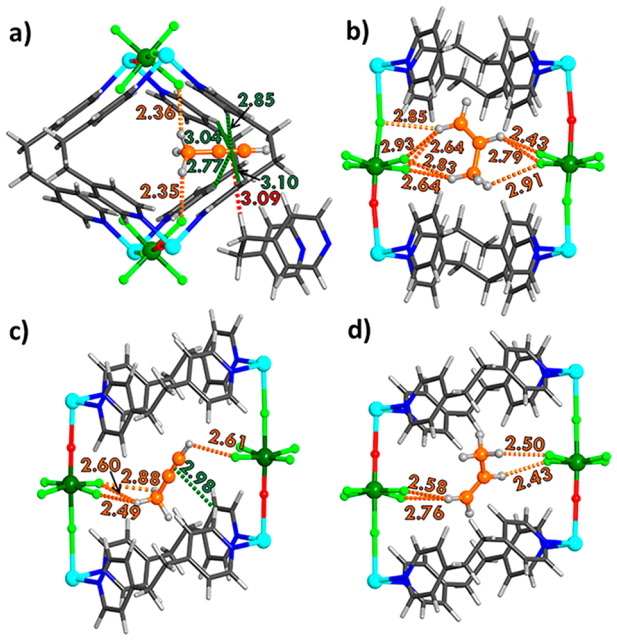

Figure 5. Binding sites of (a) C_3H_4 and (b) C_3H_6 in **sql-NbOFFIVE-bpe-Cu-AB** (a, b) and **sql-NbOFFIVE-bpe-Cu-AA** (c, d). The closest contacts (Å) between framework atoms and adsorbates are highlighted in orange for C−H···F, green for C−H···π, and red for C−H (with another framework)···π.

CONCLUSIONS

In summary, two packing polymorphs of an **sql** network with intrinsic ultramicropores, **AA** and **AB**, exhibit AAAA and ABAB packing of the **sql** layers, respectively. **AA** is isostructural with **sql-SIFSIX-bpe-Zn** and exhibits intrinsic 1D channels within each **sql** network. **AB** exhibits both intrinsic channels and extrinsic channels between the **sql** networks that arise from the different crystal packing of adjacent layers. Both polymorphs were found to display phase transformations induced by pressure and temperature. **AB** was found to be the most interesting sorbent in terms of sorption properties, as it exhibits excellent C_3H_4/C_3H_6 separation performance as indicated by a new high for C_3H_4/C_3H_6 experimental selectivity (270) and a new benchmark for polymer-grade C_3H_6 productivity (118 mmol g^{-1}) from a 1:99 C_3H_4/C_3H_6 binary mixture. Modeling studies provided insight into the selective binding sites for C_3H_4. This work has not only resulted in a new benchmark for C_3H_4 separation from C_3H_6 but also brings a new approach to pore engineering. Specifically, whereas the packing polymorphs exhibit similar surface areas, their pore chemistry, size, and shape are distinctly different.

https://doi.org/10.1021/jacs.3c03505
J. Am. Chem. Soc. 2023, 145, 11837−11845

■ ASSOCIATED CONTENT

Supporting Information

The Supporting Information is available free of charge at https://pubs.acs.org/doi/10.1021/jacs.3c03505.

Experimental and characterization details; additional figures and images; PXRD patterns; VT-PXRD patterns; TGA analysis, DVS analysis, and Sorption isotherms. (PDF)

Accession Codes

CCDC 1973753 and 2154469−2154473 contain the supplementary crystallographic data for this paper. These data can be obtained free of charge via www.ccdc.cam.ac.uk/data_request/cif, or by emailing data_request@ccdc.cam.ac.uk, or by contacting The Cambridge Crystallographic Data Centre, 12 Union Road, Cambridge CB2 1EZ, UK; fax: +44 1223 336033.

■ AUTHOR INFORMATION

Corresponding Author

Michael J. Zaworotko − *Bernal Institute, Department of Chemical Sciences, University of Limerick, Limerick V94 T9PX, Republic of Ireland;* orcid.org/0000-0002-1360-540X; Email: xtal@ul.ie

Authors

Mei-Yan Gao − *Bernal Institute, Department of Chemical Sciences, University of Limerick, Limerick V94 T9PX, Republic of Ireland;* orcid.org/0000-0001-6628-5190

Andrey A. Bezrukov − *Bernal Institute, Department of Chemical Sciences, University of Limerick, Limerick V94 T9PX, Republic of Ireland*

Bai-Qiao Song − *Bernal Institute, Department of Chemical Sciences, University of Limerick, Limerick V94 T9PX, Republic of Ireland*

Meng He − *Department of Chemistry, University of Manchester, Manchester M13 9PL, U.K.;* orcid.org/0000-0001-7373-9779

Sousa Javan Nikkhah − *Bernal Institute, Department of Chemical Sciences, University of Limerick, Limerick V94 T9PX, Republic of Ireland;* orcid.org/0000-0003-1725-4069

Shi-Qiang Wang − *Institute of Materials Research and Engineering (IMRE), Agency for Science, Technology and Research (A*STAR), 138634, Singapore;* orcid.org/0000-0003-1213-8317

Naveen Kumar − *Bernal Institute, Department of Chemical Sciences, University of Limerick, Limerick V94 T9PX, Republic of Ireland*

Shaza Darwish − *Bernal Institute, Department of Chemical Sciences, University of Limerick, Limerick V94 T9PX, Republic of Ireland;* orcid.org/0000-0001-9397-6886

Debobroto Sensharma − *Bernal Institute, Department of Chemical Sciences, University of Limerick, Limerick V94 T9PX, Republic of Ireland;* orcid.org/0000-0002-4918-0730

Chenghua Deng − *Bernal Institute, Department of Chemical Sciences, University of Limerick, Limerick V94 T9PX, Republic of Ireland*

Jiangnan Li − *Department of Chemistry, University of Manchester, Manchester M13 9PL, U.K.*

Lunjie Liu − *Department of Materials Science and Engineering, Southern University of Science and Technology, Shenzhen, Guangdong 518055, China*

Rajamani Krishna − *Van't Hoff Institute for Molecular Sciences, University of Amsterdam, 1098 XH, Amsterdam, Netherlands;* orcid.org/0000-0002-4784-8530

Matthias Vandichel − *Bernal Institute, Department of Chemical Sciences, University of Limerick, Limerick V94 T9PX, Republic of Ireland;* orcid.org/0000-0003-1592-0726

Sihai Yang − *Department of Chemistry, University of Manchester, Manchester M13 9PL, U.K.;* orcid.org/0000-0002-1111-9272

Complete contact information is available at: https://pubs.acs.org/10.1021/jacs.3c03505

Notes

The authors declare no competing financial interest.

■ ACKNOWLEDGMENTS

M.J.Z. acknowledges the support of the Science Foundation Ireland (16/IA/4624), the Irish Research Council (IRCLA/2019/167), and the European Research Council (ADG 885695). S.J.N. and M.V. acknowledge the Irish Centre for High-End Computing (ICHEC) for the provision of computational facilities and support. S.J.N. is grateful for the support by Enterprise Ireland and the European Union's Horizon 2020 research and innovation programme under the Marie Skłodowska-Curie (grant agreement no. 847402, project ID: MF20210297). We are especially grateful to ESRF for access to beamline ID22 and the Diamond Light Source for access to beamline I19, as well as the beamline scientists for their support.

■ REFERENCES

(1) Perry, J. J.; Perman, J. A.; Zaworotko, M. J. Design and synthesis of metal-organic frameworks using metal-organic polyhedra as supermolecular building blocks. *Chem. Soc. Rev.* **2009**, *38*, 1400−1417.

(2) Li, J. R.; Sculley, J.; Zhou, H. C. Metal-organic frameworks for separations. *Chem. Rev.* **2012**, *112*, 869−932.

(3) Yaghi, O. M.; O'Keeffe, M.; Ockwig, N. W.; Chae, H. K.; Eddaoudi, M.; Kim, J. Reticular synthesis and the design of new materials. *Nature* **2003**, *423*, 705−714.

(4) Furukawa, H.; Cordova, K. E.; O'Keeffe, M.; Yaghi, O. M. The Chemistry and Applications of Metal-Organic Frameworks. *Science* **2013**, *341*, 1230444.

(5) Kitagawa, S.; Kitaura, R.; Noro, S. Functional porous coordination polymers. *Angew. Chem., Int. Ed.* **2004**, *43*, 2334−2375.

(6) Sui, J.; Liu, H.; Hu, S.; Sun, K.; Wan, G.; Zhou, H.; Zheng, X.; Jiang, H. L. A General Strategy to Immobilize Single-Atom Catalysts in Metal-Organic Frameworks for Enhanced Photocatalysis. *Adv. Mater.* **2022**, *34*, 2109203.

(7) Moussa, Z.; Hmadeh, M.; Abiad, M. G.; Dib, O. H.; Patra, D. Encapsulation of curcumin in cyclodextrin-metal organic frameworks: Dissociation of loaded CD-MOFs enhances stability of curcumin. *Food Chem.* **2016**, *212*, 485−494.

(8) Mortada, B.; Matar, T. A.; Sakaya, A.; Atallah, H.; Kara Ali, Z.; Karam, P.; Hmadeh, M. Postmetalated Zirconium Metal Organic Frameworks as a Highly Potent Bactericide. *Inorg. Chem.* **2017**, *56*, 4739−4745.

(9) Das, M. C.; Xiang, S.; Zhang, Z.; Chen, B. Functional mixed metal-organic frameworks with metalloligands. *Angew. Chem., Int. Ed.* **2011**, *50*, 10510−10520.

(10) Zhu, A. X.; Yang, Q. Y.; Mukherjee, S.; Kumar, A.; Deng, C. H.; Bezrukov, A. A.; Shivanna, M.; Zaworotko, M. J. Tuning the Gate-Opening Pressure in a Switching pcu Coordination Network, X-pcu-5-Zn, by Pillar-Ligand Substitution. *Angew. Chem., Int. Ed.* **2019**, *58*, 18212−18217.

(11) Ke, T.; Wang, Q.; Shen, J.; Zhou, J.; Bao, Z.; Yang, Q.; Ren, Q. Molecular Sieving of C2 -C3 Alkene from Alkyne with Tuned

Threshold Pressure in Robust Layered Metal-Organic Frameworks. *Angew. Chem., Int. Ed.* **2020**, *59*, 12725−12730.
(12) Peng, Y. L.; Wang, T.; Jin, C.; Li, P.; Suepaul, S.; Beemer, G.; Chen, Y.; Krishna, R.; Cheng, P.; Pham, T.; Space, B.; Zaworotko, M. J.; Zhang, Z. A robust heterometallic ultramicroporous MOF with ultrahigh selectivity for propyne/propylene separation. *J. Mater. Chem. A* **2021**, *9*, 2850−2856.
(13) Jiang, Y.; Hu, J.; Wang, L.; Sun, W.; Xu, N.; Krishna, R.; Duttwyler, S.; Cui, X.; Xing, H.; Zhang, Y. Comprehensive Pore Tuning in an Ultrastable Fluorinated Anion Cross-Linked Cage-Like MOF for Simultaneous Benchmark Propyne Recovery and Propylene Purification. *Angew. Chem., Int. Ed.* **2022**, *61*, e202200947.
(14) Guo, L.; Savage, M.; Carter, J. H.; Han, X.; da Silva, I.; Manuel, P.; Rudic, S.; Tang, C. C.; Yang, S.; Schroder, M. Direct Visualization of Supramolecular Binding and Separation of Light Hydrocarbons in MFM-300(In). *Chem. Mater.* **2022**, *34*, 5698−5705.
(15) Lin, R. B.; Zhang, Z.; Chen, B. Achieving High Performance Metal-Organic Framework Materials through Pore Engineering. *Acc. Chem. Res.* **2021**, *54*, 3362−3376.
(16) Hong, A. N.; Yang, H.; Bu, X.; Feng, P. Pore space partition of metal-organic frameworks for gas storage and separation. *EnergyChem.* **2022**, *4*, 100080.
(17) Kokcam-Demir, U.; Goldman, A.; Esrafili, L.; Gharib, M.; Morsali, A.; Weingart, O.; Janiak, C. Coordinatively unsaturated metal sites (open metal sites) in metal-organic frameworks: design and applications. *Chem. Soc. Rev.* **2020**, *49*, 2751−2798.
(18) Subramanian, S.; Zaworotko, M. J. Porous Solids by Design: $[Zn(4,4'\text{-bpy})_2(SiF_6)]_n \cdot xDMF$, a Single Framework Octahedral Coordination Polymer with Large Square Channel. *Angew. Chem., Int. Ed.* **1995**, *34*, 2127−2128.
(19) Cadiau, A.; Belmabkhout, Y.; Adil, K.; Bhatt, P. M.; Pillai, R. S.; Shkurenko, A.; Martineau-Corcos, C.; Maurin, G.; Eddaoudi, M. Hydrolytically stable fluorinated metal-organic frameworks for energy-efficient dehydration. *Science* **2017**, *356*, 731−735.
(20) Song, B. Q.; Yang, Q. Y.; Wang, S. Q.; Vandichel, M.; Kumar, A.; Crowley, C.; Kumar, N.; Deng, C. H.; GasconPerez, V.; Lusi, M.; Wu, H.; Zhou, W.; Zaworotko, M. J. Reversible Switching between Nonporous and Porous Phases of a New SIFSIX Coordination Network Induced by a Flexible Linker Ligand. *J. Am. Chem. Soc.* **2020**, *142*, 6896−6901.
(21) Nugent, P.; Belmabkhout, Y.; Burd, S. D.; Cairns, A. J.; Luebke, R.; Forrest, K.; Pham, T.; Ma, S.; Space, B.; Wojtas, L.; Eddaoudi, M.; Zaworotko, M. J. Porous materials with optimal adsorption thermodynamics and kinetics for CO_2 separation. *Nature* **2013**, *495*, 80−84.
(22) Chen, K. J.; Madden, D. G.; Mukherjee, S.; Pham, T.; Forrest, K. A.; Kumar, A.; Space, B.; Kong, J.; Zhang, Q. Y.; Zaworotko, M. J. Synergistic sorbent separation for one-step ethylene purification from a four-component mixture. *Science* **2019**, *366*, 241−246.
(23) Cui, X.; Chen, K.; Xing, H.; Yang, Q.; Krishna, R.; Bao, Z.; Wu, H.; Zhou, W.; Dong, X.; Han, Y.; Li, B.; Ren, Q.; Zaworotko, M. J.; Chen, B. Pore chemistry and size control in hybrid porous materials for acetylene capture from ethylene. *Science* **2016**, *353*, 141−144.
(24) Wang, J.; Zhang, Y.; Su, Y.; Liu, X.; Zhang, P.; Lin, R. B.; Chen, S.; Deng, Q.; Zeng, Z.; Deng, S.; Chen, B. Fine pore engineering in a series of isoreticular metal-organic frameworks for efficient C_2H_2/CO_2 separation. *Nat. Commun.* **2022**, *13*, 200.
(25) Sensharma, D.; O'Hearn, D. J.; Koochaki, A.; Bezrukov, A. A.; Kumar, N.; Wilson, B. H.; Vandichel, M.; Zaworotko, M. J. The First Sulfate-Pillared Hybrid Ultramicroporous Material, SOFOUR-1-Zn, and Its Acetylene Capture Properties. *Angew. Chem., Int. Ed.* **2022**, *61*, e202116145.
(26) Scott, H. S.; Shivanna, M.; Bajpai, A.; Chen, K.-J.; Madden, D. G.; Perry, J. J., IV; Zaworotko, M. J. Enhanced Stability toward Humidity in a Family of Hybrid Ultramicroporous Materials Incorporating Cr2O72− Pillars. *Cryst. Growth Des.* **2017**, *17*, 1933−1937.
(27) Shivanna, M.; Otake, K. I.; Song, B. Q.; van Wyk, L. M.; Yang, Q. Y.; Kumar, N.; Feldmann, W. K.; Pham, T.; Suepaul, S.; Space, B.; Barbour, L. J.; Kitagawa, S.; Zaworotko, M. Benchmark acetylene binding affinity and separation through induced fit in a flexible hybrid ultramicroporous material. *Angew. Chem., Int. Ed.* **2021**, *60*, 20383−20390.
(28) Lin, R. B.; Xiang, S.; Xing, H.; Zhou, W.; Chen, B. Exploration of porous metal-organic frameworks for gas separation and purification. *Coord. Chem. Rev.* **2019**, *378*, 87−103.
(29) Zhao, X.; Wang, Y.; Li, D. S.; Bu, X.; Feng, P. Metal-Organic Frameworks for Separation. *Adv. Mater.* **2018**, *30*, 1705189.
(30) Barnett, B. R.; Gonzalez, M. I.; Long, J. R. Recent Progress Towards Light Hydrocarbon Separations Using Metal-Organic Frameworks. *Trends Chem.* **2019**, *1*, 159−171.
(31) Lan, T.; Li, L.; Chen, Y.; Wang, X.; Yang, J.; Li, J. Opportunities and critical factors of porous metal-organic frameworks for industrial light olefins separation. *Mater. Chem. Front.* **2020**, *4*, 1954−1984.
(32) Wang, H.; Liu, Y.; Li, J. Designer Metal-Organic Frameworks for Size-Exclusion-Based Hydrocarbon Separations: Progress and Challenges. *Adv. Mater.* **2020**, *32*, 2002603.
(33) Pei, J.; Shao, K.; Zhang, L.; Wen, H. M.; Li, B.; Qian, G. Current Status of Microporous Metal-Organic Frameworks for Hydrocarbon Separations. *Top. Curr. Chem.* **2019**, *377*, 33.
(34) Li, H.; Li, L.; Lin, R.-B.; Zhou, W.; Zhang, Z.; Xiang, S.; Chen, B. Porous metal-organic frameworks for gas storage and separation: Status and challenges. *EnergyChem.* **2019**, *1*, 100006.
(35) Lin, R. B.; Xiang, S.; Zhou, W.; Chen, B. Microporous Metal-Organic Framework Materials for Gas Separation. *Chem.* **2020**, *6*, 337.
(36) Wang, B.; Xie, L. H.; Wang, X.; Liu, X. M.; Li, J.; Li, J. R. Applications of metal-organic frameworks for green energy and environment: New advances in adsorptive gas separation, storage and removal. *Green Energy Environ.* **2018**, *3*, 191−228.
(37) Wang, S. Q.; Mukherjee, S.; Zaworotko, M. J. Spiers Memorial Lecture: Coordination networks that switch between nonporous and porous structures: an emerging class of soft porous crystals. *Faraday Discuss.* **2021**, *231*, 9−50.
(38) Li, L.; Wen, H. M.; He, C.; Lin, R. B.; Krishna, R.; Wu, H.; Zhou, W.; Li, J.; Li, B.; Chen, B. A Metal-Organic Framework with Suitable Pore Size and Specific Functional Sites for the Removal of Trace Propyne from Propylene. *Angew. Chem., Int. Ed.* **2018**, *57*, 15183−15188.
(39) Shekhah, O.; Belmabkhout, Y.; Chen, Z.; Guillerm, V.; Cairns, A.; Adil, K.; Eddaoudi, M. Made-to-order metal-organic frameworks for trace carbon dioxide removal and air capture. *Nat. Commun.* **2014**, *5*, 4228.
(40) Shekhah, O.; Belmabkhout, Y.; Adil, K.; Bhatt, P. M.; Cairns, A. J.; Eddaoudi, M. A facile solvent-free synthesis route for the assembly of a highly CO_2 selective and H_2S tolerant NiSIFSIX metal-organic framework. *Chem. Commun.* **2015**, *51*, 13595−13598.
(41) Wang, J.; Zhang, Y.; Zhang, P.; Hu, J.; Lin, R. B.; Deng, Q.; Zeng, Z.; Xing, H.; Deng, S.; Chen, B. Optimizing Pore Space for Flexible-Robust Metal-Organic Framework to Boost Trace Acetylene Removal. *J. Am. Chem. Soc.* **2020**, *142*, 9744−9751.
(42) Shen, J.; He, X.; Ke, T.; Krishna, R.; van Baten, J. M.; Chen, R.; Bao, Z.; Xing, H.; Dinca, M.; Zhang, Z.; Yang, Q.; Ren, Q. Simultaneous interlayer and intralayer space control in two-dimensional metal-organic frameworks for acetylene/ethylene separation. *Nat. Commun.* **2020**, *11*, 6259.
(43) Lin, R. B.; Li, L. B.; Wu, H.; Arman, H.; Li, B.; Lin, R. G.; Zhou, W.; Chen, B. L. Optimized Separation of Acetylene from Carbon Dioxide and Ethylene in a Microporous Material. *J. Am. Chem. Soc.* **2017**, *139*, 8022−8028.
(44) Suen, M. C.; Chan, Z. K.; Chen, J. D.; Wang, J. C.; Hung, C. H. Syntheses and structures of three new coordination polymers generated from the flexible 1,3-bis(4-pyridyl)propane ligand and zinc salts. *Polyhedron* **2006**, *25*, 2325−2332.
(45) Cadiau, A.; Adil, K.; Bhatt, P. M.; Belmabkhout, Y.; Eddaoudi, M. A metal-organic framework-based splitter for separating propylene from propane. *Science* **2016**, *353*, 137−140.
(46) Zeng, H.; Xie, M.; Wang, T.; Wei, R.-J.; Xie, X.-J.; Zhao, Y.; Lu, W.; Li, D. Orthogonal-array dynamic molecular sieving of propylene/propane mixtures. *Nature* **2021**, *595*, 542−548.

https://doi.org/10.1021/jacs.3c03505
J. Am. Chem. Soc. 2023, 145, 11837−11845

(47) Gao, M. Y.; Song, B. Q.; Sensharma, D.; Zaworotko, M. J. Crystal engineering of porous coordination networks for C3 hydrocarbon separation. *SmartMat* **2021**, *2*, 38−55.
(48) Yang, L.; Cui, X.; Yang, Q.; Qian, S.; Wu, H.; Bao, Z.; Zhang, Z.; Ren, Q.; Zhou, W.; Chen, B.; Xing, H. A Single-Molecule Propyne Trap: Highly Efficient Removal of Propyne from Propylene with Anion-Pillared Ultramicroporous Materials. *Adv. Mater.* **2018**, *30*, 1705374.
(49) Peng, Y. L.; He, C.; Pham, T.; Wang, T.; Li, P.; Krishna, R.; Forrest, K. A.; Hogan, A.; Suepaul, S.; Space, B.; Fang, M.; Chen, Y.; Zaworotko, M. J.; Li, J.; Li, L.; Zhang, Z.; Cheng, P.; Chen, B. Robust Microporous Metal-Organic Frameworks for Highly Efficient and Simultaneous Removal of Propyne and Propadiene from Propylene. *Angew. Chem., Int. Ed.* **2019**, *58*, 10209−10214.
(50) Heier, K. R.; Poeppelmeier, K. R. Reinvestigation of $CuNbOF_5 \cdot 4H_2O$. *J. Solid State Chem.* **1997**, *133*, 576−579.
(51) Lin, M. J.; Jouaiti, A.; Pocic, D.; Kyritsakas, N.; Planeix, J. M.; Hosseini, M. W. Molecular tectonics: tubular crystals with controllable channel size and orientation. *Chem. Commun.* **2010**, *46*, 112−114.
(52) Spek, A. L. Single-crystal structure validation with the program PLATON. *J. Appl. Crystallogr.* **2003**, *36*, 7−13.
(53) Yang, L.; Cui, X.; Zhang, Z.; Yang, Q.; Bao, Z.; Ren, Q.; Xing, H. An Asymmetric Anion-Pillared Metal-Organic Framework as a Multisite Adsorbent Enables Simultaneous Removal of Propyne and Propadiene from Propylene. *Angew. Chem., Int. Ed.* **2018**, *57*, 13145−13149.
(54) Li, J.; Bhatt, P. M.; Li, J.; Eddaoudi, M.; Liu, Y. Recent Progress on Microfine Design of Metal-Organic Frameworks: Structure Regulation and Gas Sorption and Separation. *Adv. Mater.* **2020**, *32*, 2002563.
(55) Cui, W. G.; Hu, T. L.; Bu, X. H. Metal-Organic Framework Materials for the Separation and Purification of Light Hydrocarbons. *Adv. Mater.* **2020**, *32*, 1806445.
(56) Qian, S.; Hu, J.; Wang, X.; Yang, L.; Suo, X.; Wang, Z.; Cui, X.; Xing, H. Anion-pillared microporous material incorporated mixed-matrix fiber adsorbents for removal of trace propyne from propylene. *AIChE J.* **2023**, e18091.
(57) Yang, Q. Y.; Lama, P.; Sen, S.; Lusi, M.; Chen, K. J.; Gao, W. Y.; Shivanna, M.; Pham, T.; Hosono, N.; Kusaka, S.; Perry, J. J. t.; Ma, S.; Space, B.; Barbour, L. J.; Kitagawa, S.; Zaworotko, M. J. Reversible Switching between Highly Porous and Nonporous Phases of an Interpenetrated Diamondoid Coordination Network That Exhibits Gate-Opening at Methane Storage Pressures. *Angew. Chem., Int. Ed.* **2018**, *57*, 5684−5689.
(58) Li, L.; Lin, R. B.; Krishna, R.; Wang, X.; Li, B.; Wu, H.; Li, J.; Zhou, W.; Chen, B. Flexible-Robust Metal-Organic Framework for Efficient Removal of Propyne from Propylene. *J. Am. Chem. Soc.* **2017**, *139*, 7733−7736.
(59) Yang, L.; Cui, X.; Zhang, Y.; Yang, Q.; Xing, H. A highly sensitive flexible metal-organic framework sets a new benchmark for separating propyne from propylene. *J. Mater. Chem. A* **2018**, *6*, 24452−24458.
(60) Gutierrez-Sevillano, J. J.; Calero, S.; Krishna, R. Separation of benzene from mixtures with water, methanol, ethanol, and acetone: highlighting hydrogen bonding and molecular clustering influences in CuBTC. *Phys. Chem. Chem. Phys.* **2015**, *17*, 20114−20124.
(61) Gutiérrez-Sevillano, J. J.; Calero, S.; Krishna, R. Selective Adsorption of Water from Mixtures with 1-Alcohols by Exploitation of Molecular Packing Effects in CuBTC. *J. Phys. Chem. C* **2015**, *119*, 3658−3666.
(62) Pan, H.; Ritter, J. A.; Balbuena, P. B. Examination of the Approximations Used in Determining the Isosteric Heat of Adsorption from the Clausius-Clapeyron Equation. *Langmuir* **1998**, *14*, 6323−6327.
(63) Krishna, R. Metrics for Evaluation and Screening of Metal-Organic Frameworks for Applications in Mixture Separations. *ACS Omega* **2020**, *5*, 16987−17004.
(64) Krishna, R. Methodologies for screening and selection of crystalline microporous materials in mixture separations. *Sep. Purif. Technol.* **2018**, *194*, 281−300.
(65) Krishna, R. The Maxwell-Stefan description of mixture diffusion in nanoporous crystalline materials. *Microporous Mesoporous Mater.* **2014**, *185*, 30−50.
(66) Krishna, R. Methodologies for evaluation of metal-organic frameworks in separation applications. *RSC Adv.* **2015**, *5*, 52269−52295.
(67) Krishna, R. Screening metal-organic frameworks for mixture separations in fixed-bed adsorbers using a combined selectivity/capacity metric. *RSC Adv.* **2017**, *7*, 35724−35737.
(68) Chai, Y.; Han, X.; Li, W.; Liu, S.; Yao, S.; Wang, C.; Shi, W.; da-Silva, I.; Manuel, P.; Cheng, Y.; Daemen, L. D.; Ramirez-Cuesta, A. J.; Tang, C. C.; Jiang, L.; Yang, S.; Guan, N.; Li, L. Control of zeolite pore interior for chemoselective alkyne/olefin separations. *Science* **2020**, *368*, 1002−1006.
(69) Jiang, Y.; Wang, L.; Yan, T.; Hu, J.; Sun, W.; Krishna, R.; Wang, D.; Gu, Z.; Liu, D.; Cui, X.; Xing, H.; Zhang, Y. Insights into the thermodynamic-kinetic synergistic separation of propyne/propylene in anion pillared cage MOFs with entropy-enthalpy balanced adsorption sites. *Chem. Sci.* **2023**, *14*, 298−309.
(70) Gao, M. Y.; Sensharma, D.; Bezrukov, A. A.; Andaloussi, Y. H.; Darwish, S.; Deng, C.; Vandichel, M.; Zhang, J.; Zaworotko, M. J. A Robust Molecular Porous Material for C_2H_2/CO_2 Separation. *Small* **2023**, *19*, e2206945.
(71) Wang, J. X.; Liang, C.-C.; Gu, X.-W.; Wen, H.-M.; Jiang, C.; Li, B.; Qian, G.; Chen, B. Recent advances in microporous metal-organic frameworks as promising adsorbents for gas separation. *J. Mater. Chem. A* **2022**, *10*, 17878−17916.
(72) Li, X.; Bian, H.; Huang, W.; Yan, B.; Wang, X.; Zhu, B. A review on anion-pillared metal-organic frameworks (APMOFs) and their composites with the balance of adsorption capacity and separation selectivity for efficient gas separation. *Coord. Chem. Rev.* **2022**, *470*, 214714.
(73) Ebadi Amooghin, A.; Sanaeepur, H.; Luque, R.; Garcia, H.; Chen, B. Fluorinated metal-organic frameworks for gas separation. *Chem. Soc. Rev.* **2022**, *51*, 7427−7508.

https://doi.org/10.1021/jacs.3c03505
J. Am. Chem. Soc. 2023, 145, 11837−11845